catalysts

MDPI

Article

Hydrogen Production from Aqueous Methanol Solutions Using Ti–Zr Mixed Oxides as Photocatalysts under UV Irradiation

Alejandro Pérez-Larios [1,2,*], Jose L. Rico [3], Luis M. Anaya-Esparza [1], O.A. González Vargas [4], Napoleón González-Silva [1] and Ricardo Gómez [2]

1 Division of Agricultural Sciences and Engineering, Campus Los Altos, University of Guadalajara, Av. Rafael Casillas Aceves 1200, Tepatitlán de Morelos, Jalisco 47600, Mexico; l_m_ae@hotmail.com (L.M.A.-E.); napoleon.gonzalez@cualtos.udg.mx (N.G.-S.)

2 Department of Chemistry, Iztapalapa Unit, Metropolitan Autonomous University, Av. San Rafael Atlixco No 189, Mexico City 09340, Mexico; gomr@xanum.uam.mx

3 Department of Chemical Engineering, Laboratorio de Catálisis, Universidad Michoacana de San Nicolás de, Morelia 58060, Mexico; jlrico@umich.mx

4 Departamento de Ingeniería en Control y Automatización, Escuela Superior de Ingeniería Mecánica y Eléctrica-Zacatenco, Instituto Politécnico Nacional, UPALM, Av. Politécnico S/N, Col. Zacatenco, Alcaldía Gustavo A. Madero, Ciudad de México 07738, Mexico; ogonzalezv@ipn.mx

* Correspondence: alarios@cualtos.udg.mx

Received: 10 October 2019; Accepted: 5 November 2019; Published: 8 November 2019

Abstract: The synthesis and characterisation of Ti–Zr mixed oxides containing 1 to 10 wt.% of Zr is herein reported. In addition, the samples were tested as photocatalysts in the generation of hydrogen from aqueous methanol solutions. The solids were prepared by sol-gel and then characterised by X-ray diffraction, high resolution electron microscopy, X-ray photoelectron spectroscopy, physisorption of nitrogen, scanning electron microscopy, UV-vis and Raman spectroscopies. The results show the presence of anatase as a predominant structure and the oxides present larger specific surface areas than that of pure titania. A maximum value of 168 m^2/g was determined for the sample with 5 wt.% of zirconium. The calculated band gap energies varied from 3.05 to 3.15 eV. It was observed that the greater the zirconium content in the solid, the higher the generation rate of hydrogen when testing the Ti–Zr solids as photocatalysts. Under our experimental conditions, the best catalyst, Ti–Zr oxide with 10 wt.% Zr, showed a production rate of 2100 µmol of H_2/h which was about tenfold higher than that observed for pure titania.

Keywords: hydrogen production; photocatalysis; mixed oxide; nanocomposite; photocatalysts

1. Introduction

Hydrogen is considered one of the most promising fuels for the future. However, most of the available hydrogen in the world is produced from the reforming of methane [1]. Carbon monoxide generated from this process eventually contaminates and contributes to the high level of CO_2 in the atmosphere. Contrarily, the photocatalytic generation of hydrogen from water only produces O_2 and H_2 and it is therefore a very attractive and promising process. However, for a photocatalytic process to be economical and sustainable, the development of efficient catalysts and the use of a renewable energy source are required [2]. Since the pioneering work published by Fujishima and Honda on the photocatalytic generation of hydrogen from water [3], extensive research on this subject has been observed worldwide.

Commonly, efficient photocatalysts contain either transition-metal cations with a d^0 electronic configuration, such as Ti^{4+}, Zr^{4+}, Nb^{5+}, Ta^{5+}, W^{6+} and Mo^{6+}, or typical metal cations with d^{10} electronic configuration such as Ga^{3+}, In^{3+}, Sn^{4+}, Ge^{4+}, Sb^{5+} as principal cation components, and their empty d or sp orbitals form the bottom of the respective conduction bands [4–6]. Due to its catalytic activity, low toxicity, stability and availability, titanium oxide is one of the most utilised photocatalysts [7,8]. However, the production of hydrogen from water under TiO_2 and UV irradiation is a low efficiency process, due to the rapid recombination of the light-induced electrons and holes [9]. The addition of other elements into titania are therefore aimed at enhancing the photocatalytic activity, i.e., Cu, Pt, Au and N among others [10]. Although the incorporation of sacrificial reactants improves the evolution of hydrogen by forming an electron donor [9], the generation of byproducts is undesirable.

We have previously reported the addition of Mn, Zn, Cu-Zr into titania and the catalysts were tested in the photocatalytic splitting of water [11–13]. The aim of the present report was to further explore the synthesis and catalytic behaviour of a series of bimetallic Ti–Zr mixed oxides as photocatalysts in the generation of hydrogen from methanol–water solutions under UV irradiation.

2. Results and Discussion

Figure 1 presents some micrographs of the samples synthetised in this work. All catalysts revealed similar morphological features. The images are comprised of agglomerates and no apparent differences are noticed when zirconium was incorporated into titania.

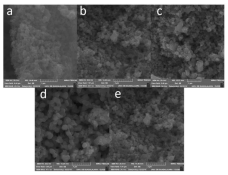

Figure 1. Morphology of samples obtained by SEM, (**a**): TiO_2, (**b**): TZr-1, (**c**): TZr-3, (**d**): TZr-5, (**e**): TZr-10.

The specific surface areas of catalysts after calcination at 500 °C for 5 h are reported in Table 1. A clear increase in area is observed when zirconium is augmented until the TZr-5 sample and a slight decrease was noticed for TZr-10. The largest area (157 m^2/g) was determined for TZr-5. Figure 2 shows the isotherms of the metal oxides after calcination which correspond to type IV and H1 hysteresis. The synthetised solids are mesoporous materials with uniform porosity. An insert in Figure 2 shows that the solids present a narrow pore size distribution. According to the zirconium content, the mean pore size increases as the zirconium content augments, reaching a maximum and then decreases for TZr-10 (Table 1).

Table 1. Textural properties, band gap (Eg) and H_2 production rates of the Ti–Zr samples.

Zr	$S_{(BET)}$	Mean Pore Size	Eg	Cell Parameter a	Crystallite Size	H_2 Production
(wt.%)	(m^2/g)	(nm)	(eV)	(nm)	(nm)	(μmoL/h)
1.0	91	5.6	3.05	0.560	1.76	387
3.0	147	7.7	3.14	0.580	0.98	900
5.0	157	7.8	3.20	0.660	0.96	1600
10.0	138	9.5	3.15	0.780	1.36	2100
TiO_2	64	6.5	3.20	0.377	5.02	190

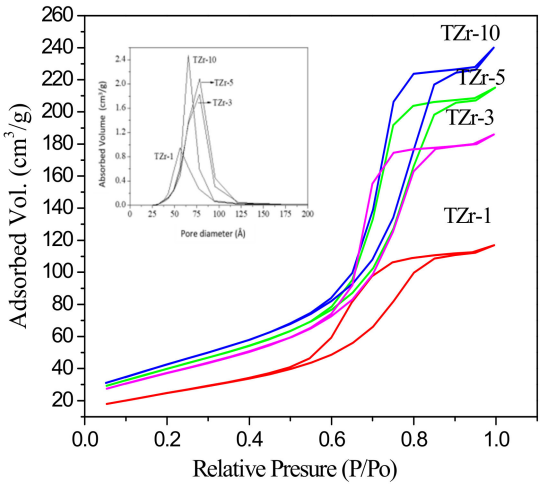

Figure 2. N_2 adsorption-desorption isotherms of the Ti–Zr oxides.

Figure 3 shows the XRD patterns of samples after calcination at 500 °C. The pattern of pure titania with diffractions at 25.4°, 38°, 48°, 54°, 63° 2θ are assigned to the anatasa crystalline phase (JCPDD: 21-1272) and corresponds to the (101), (112), (200), (211) and (204) planes, respectively. It can be noticed that anatase is the predominant structure in all Ti–Zr samples. In our experiments, the Zr/Ti atomic ratios varied from 0.0053 to 0.05843 for samples with 1 to 10 wt.% Zr, respectively. These ratios are below the value of 0.075 which represents the maximum solubility of Zr^{4+} into sol-gel titania matrix reported by Yang et al. [14]. Segregation of Zr^{4+} is expected when higher Zr/Ti ratios are used. It is therefore anticipated that segregation of Zr^{4+} was absent during our synthesis. Signals assigned to ZrO_2 and $ZrTiO_4$ in the XRD patterns were unnoticed. Furthermore, it can be indeed observed that the incorporation of Zr^{4+} into titania modifies the pure anatase pattern. A shift to lower angles in the positions of the diffraction signals of the Zr-Ti samples compared to that of pure titania is clearly observed, which is an experimental evidence of the incorporation of Zr into the titania lattice. Chang and Doong reported similar variation in the XRD patterns when doping titania with zirconium [15]. However, their Ti–Zr oxides were synthetized by nonhydrolytic sol-gel synthesis at high temperature. Gómez-Avilés et al. also noticed a shift to lower angles in the diffraction signals of Ti–Zr samples with low zirconium content compared to the peaks of pure titania [16]. As expected, the incorporation of Zr^{4+} into the lattice of titania modifies the unit cell parameter **a** as can be seen in Table 1. Such variations are attributed to the difference in the ionic radii between Ti and Zr which is equal to 74.5 and 86 pm, respectively. The average crystallite size (d) reported in Table 1, was determined from the XRD patterns, using the Scherrer equation:

$$D = k\lambda/(w \cos\theta)$$

where k is a constant equal to 0.94; λ is the wavelength of the radiation (equal to 1.5405 Å for a Cu Kα radiation source); θ is the angle of the considered Bragg reflection and w is the width at half maximum (FWHM) of the XRD diffraction [17]. It is also noticed in this table that the crystallite size decreases as a function of the zirconium content. Moreover, the XRD patterns show a decrease in crystallinity as the Zr content in samples augments.

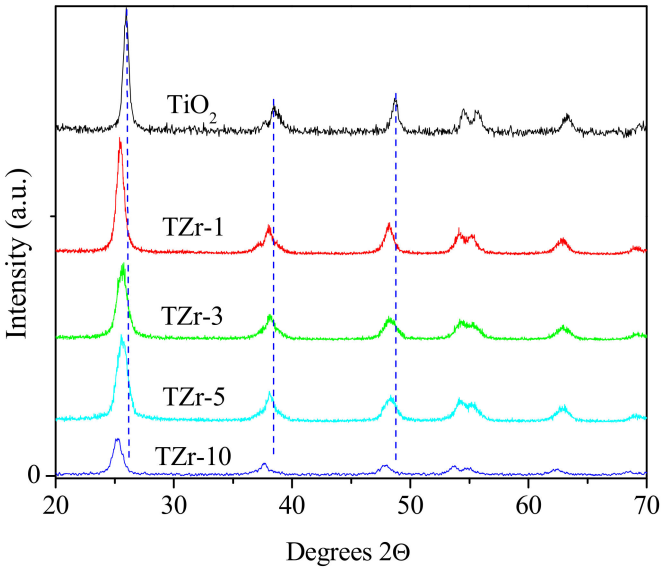

Figure 3. X-ray diffraction patterns of the Ti–Zr catalysts.

Raman spectra of the Ti–Zr oxides with various loadings of zirconium are presented in Figure 4. The Raman active mode signals at 145, 395, 513, 640 cm^{-1} and a small shoulder at about 198 cm^{-1} are characteristic of the anatase crystalline phase [18]. The signal at about 513 cm^{-1} is comprised of two overlapped peaks [19]. The broadening of the peaks increased as the zirconium content augmented but no other signals related to ZrO_2 were observed. It is expected that the incorporation of Zr into the titania lattice produces a change in the oxygen coordination and, as a consequence, defects could be created in the final structure. Moreover, it is known that the presence of defects in the crystal structure results in the broadening of the Raman modes and in a shift in the positions of the picks of the spectra [20]. The broadening was observed in the present study but not the shift. We believe that widen in the Raman signals result from the incorporation of Zr into that titania lattice. However, it is possible that the broadening could be due to the quantum size effect, present in semiconductors when the crystalline size is less than 10 nm [21,22].

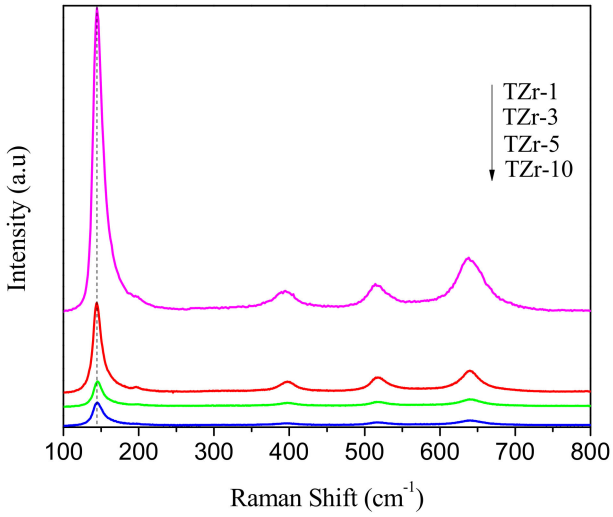

Figure 4. Raman spectra of the Ti–Zr samples.

The UV-vis spectra of TiO_2 and the Ti–Zr samples synthetized by sol-gel were acquired after calcination at 500 °C. The adsorption at about 359 nm is characteristic of the highly disperse anatase. With the increase in Zr loading, a shift in the absorption edge onset to shorter wavenumbers is clearly observed, in agreement with other reports in the literature [23]. This shift was expected since pure ZrO_2 shows a band gap energy of about 5 eV [24]. The acquired diffuse reflectance spectra were then used to obtain the Kubelka–Munk function, *F(R)*, with the aim to calculate the band gap energies. The determination is based on the following equation:

$$hv\,F(R) = (Ahv - Eg)^{\frac{n}{2}}$$

where *Eg* is the band gap energy; *hv* is the photon energy (*h* is the Plank's constant and *v* the frequency of the incident photons); A is a proportional constant. The value of *n* is determined accordingly to the type of optical transition, being $n = 1$ or 4 for direct or indirect transition, respectively [25]. In the case of TiO_2 and ZrO_2, which are indirect band semiconductors, the value of *n* is equal to 4. The band gap energies were determined from the plot of the *Ahv* versus energy by drawing a tangent line in the linear section of each spectrum and extrapolating to the horizontal axis, Figure 5. The point of interception represents the value of the band gap energy for each sample. The calculated values are presented in Table 1.

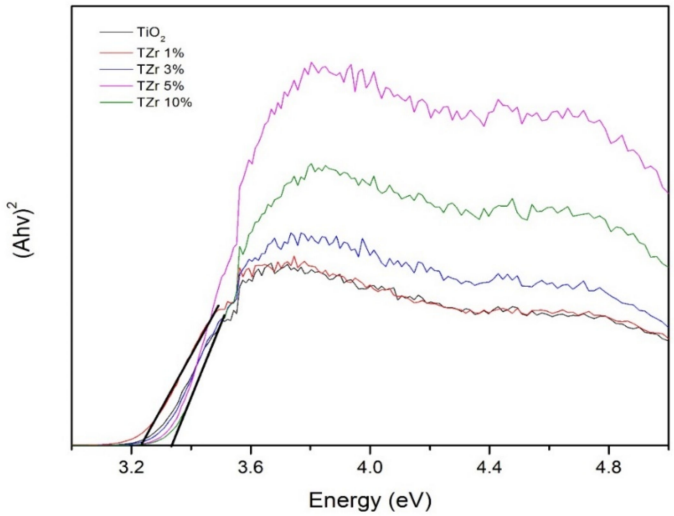

Figure 5. Determination of the band gap energies for TiO_2 and Ti–Zr samples.

To further characterise the surface of the Ti–Zr samples, XPS spectra were acquired. Figure 6 exhibits the spectra of the calcined TZr-1 and TZr-10, whereas those for TZr-1, TZr-3, TZr-5 were similar and omitted. In addition, Table 2 resumes the surface composition determined by XPS. An average of three measurements is presented in Figure 6. For deconvolution of the spectra, the mixed Gaussian-Lorentzian function and the Shirley background subtraction were utilised. The doublet observed for Zr at 181.6 and 184.5 eV corresponds to Zr $3d_{5/2}$ and Zr $3d_{3/2}$ spin-orbit splitting, respectively [26].

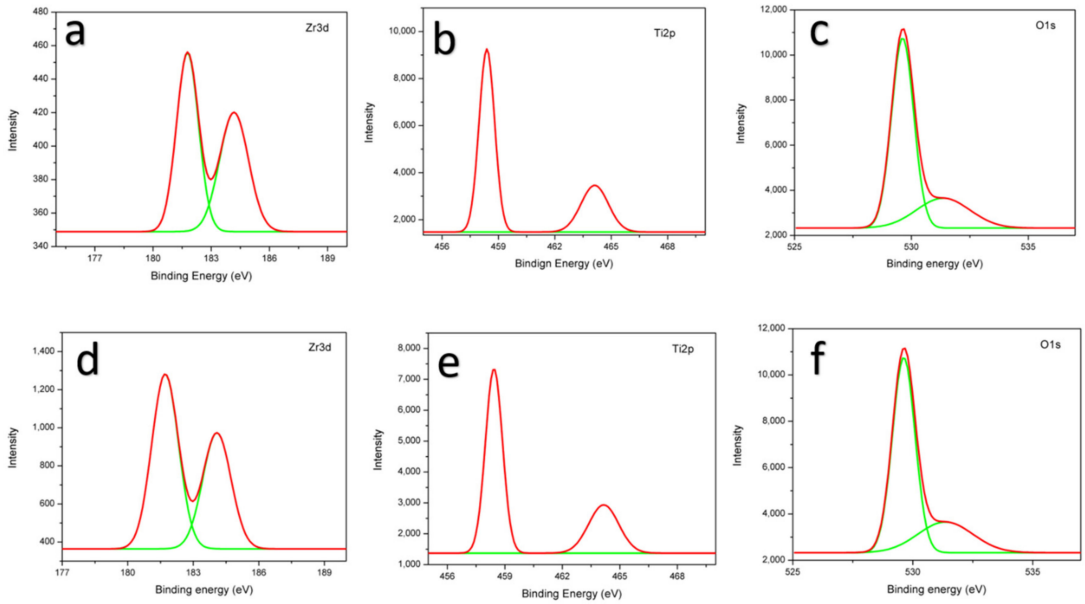

Figure 6. XPS spectra of TZr-1 (**a**–**c**) and TZr-10 (**d**–**f**) for Zr 3d, Ti 2p and O 1s.

Table 2. Superficial atomic composition of Ti 2p, Zr 3d and O 1s in TZr samples determined by XPS.

Sample	Composition						
	Ti 2p, at.%	Zr 3d, at.%	O 1s, at.%	Ti, wt.%	Zr, wt.%	O, wt.%	O 1s/(Ti 2p + Zr 3d)
TZr-1	37.8	1.0	61.3	54.6	1.0	44.40	1.58
TZr-3	36.9	1.2	61.9	53.55	2.5	43.95	1.62
TZr-5	36.2	1.9	62.0	52.15	5.0	42.85	1.63
TZr-10	35.8	2.9	61.4	47.95	9.0	43.05	1.58

The XPS Ti 2p spectra for pure titania consist of two signals with binding energies at 458 and 464 eV [27]. The Ti 2p peaks for TZr-1 reported in Figure 6 are located at 458.39 and 464.09 eV whereas those for TZr-10 at 458.42 and 464.12 eV showed a shift to higher energies compared to pure titania, indicating the incorporation of Zr into titania. These results are in agreement with the XRD observations. The shift in energy after doping was also reported by other authors for different samples [28].

The deconvolution of the O 1s spectra, presented in Figure 6, shows two peaks with binding energies at 532 and 529 eV, which correspond to surface MeOH defects and lattice oxygen, respectively [29]. The atomic percentage for O 1s reported in Table 2, comprises both signals, at 532 eV and 529 eV.

The low O1s/(Ti2p + Zr3d) ratios in the right column of Table 2 indicate a confirmation of the presence of oxygen vacancies in the solids, resulted after incorporation of Zr [30]. Such a presence of oxygen vacancies proves the existence of sub-stoichiometric metal oxides in our catalysts. It is worth commenting that Zr cation in ZrO_2 is energetically very difficult to reduce [31,32]. The charge state of zirconium is expected to be either 0 as in the case of metal, or +4 as in ZrO_2. However, Ma et al. demonstrated that the formation of Zr^{1+}, Zr^{2+} and Zr^{3+} is also possible. The authors found that the presence of a strong electrical field and the minimisation of interfacial energy can induce the formation of sub-stoichiometric oxides [33].

HRTEM images of the TZr-1 and TZr-10 photocatalysts are shown in Figure 7.

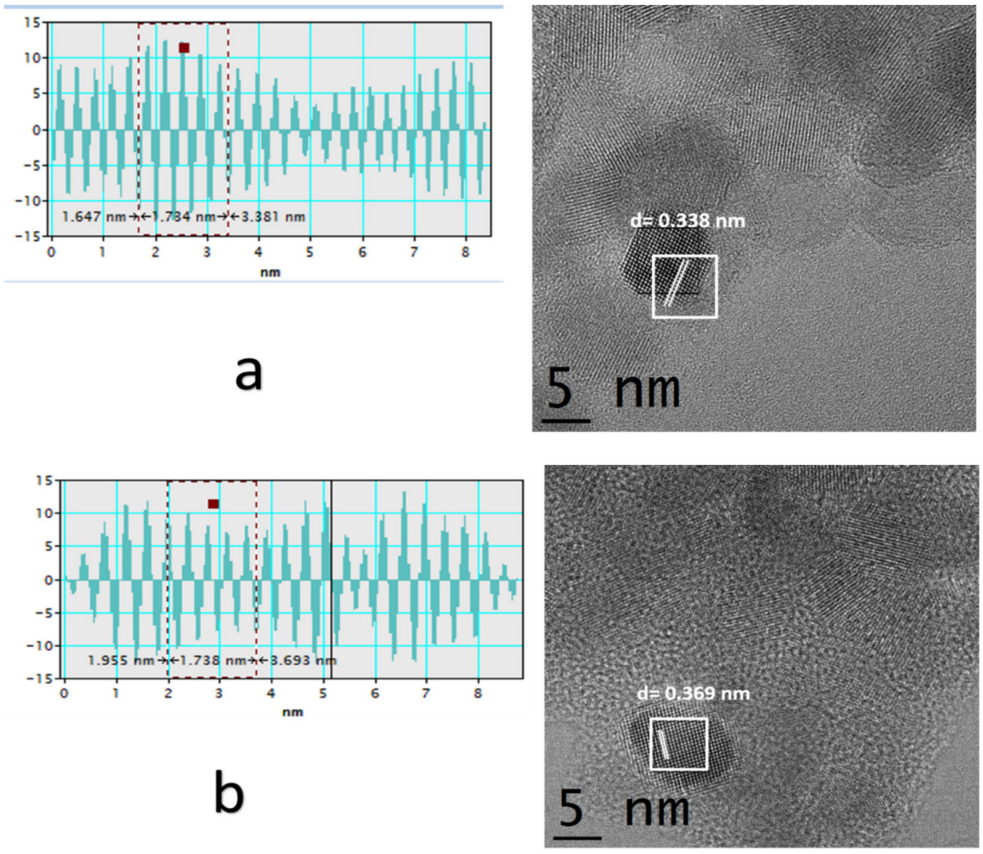

Figure 7. HRTEM images for TZr-1 (**a**) and TZr-10 (**b**).

The images show lattice fringes of the surface and indicate an interlayer spacing of 0.338 and 0.369 nm for the T-Zr samples containing 1 and 10 wt.% of zirconium, respectively. Anatase presents an interlayer d-spacing of 0.354 nm for the (101) crystalline plane. The differences in d-spacing between the doped and pure titania confirm the incorporation of zirconium into the titania structure. The results are also consistent with those obtained from the XRD analysis.

3. Photocatalytic Reactions

Before testing the Ti–Zr catalysts in the splitting of water an experiment was performed using pure titania as photocatalyst, UV irradiation and pure water as a reactant. Hydrogen was not evolved during this experiment, highlighting the importance of methanol as a sacrificial reactant.

It is known that the incidence of light of energy equal or greater than the band gap on any *n*-type of semiconducting materials results in intrinsic ionization over the band gap, producing electrons in the conduction band and electron holes in the valence band of the material. This generation can be represented as follows:

$$4h\nu \rightarrow 4e + 4h^{+}$$

The generated electron holes are capable of breaking the bonds of water producing oxygen and hydrogen ions. Furthermore, the light-induced electrons react with the hydrogen ions to produce hydrogen:

$$2H_2O + 4h^{+} \rightarrow O_2 + 4H^{+}$$

$$4H^{+} + 4h^{+} \rightarrow 2H_2$$

For the photocatalytic splitting of water to occur, the energy of the incidence photon must be at least of 1.23 eV [34], whereas methanol photooxidation requires and energy of 0.7 eV [35]. Methanol

was selected as a suitable scavenger reactant to improve the generation of hydrogen, as reported in the literature [9]. The oxidation of methanol on a photocatalyst can be represented as follows:

$$CH_3OH + H^+ \rightarrow HCOH + H_2$$

$$HCOH + H_2O + H^+ \rightarrow HCOOH + H_2$$

$$HCOOH + H^+ \rightarrow CO_2 + H_2$$

The overall photocatalytic reaction is therefore: $CH_3OH + H_2O \rightarrow 3H_2 + CO_2$

Figure 8 shows the photocatalytic production of hydrogen from an aqueous methanol solution as a function of the irradiation time. It can be noticed that the evolution of hydrogen increases as the zirconium content in catalysts augments. Consequently, the highest photocatalytic activity was observed for the TZr-10 sample. From these results and assuming a linear behaviour, a constant rate of 190 μmoL of H_2/h was determined for pristine titania, whereas values of 387, 900, 1600 and 2100 μmoL/h were measures for samples with 1, 3, 5 and 10 wt.% of zirconium, respectively. It is also expected that the large surface areas derived from the use of zirconium, Table 1, also enhance photocatalytic activity. Figure 8 also shows that among the synthetised catalysts, pure TiO_2 produces the lowest amount of hydrogen, which can be explained by considering the rapid recombination of the light-induced electron and electron holes in this material resulting in the formation of water and consequentially, the smallest amount of hydrogen [36].

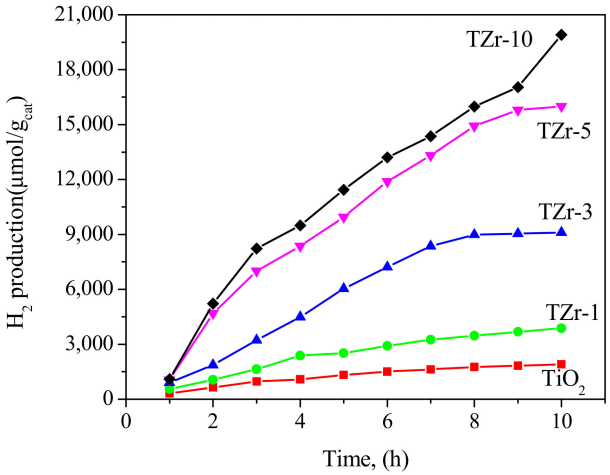

Figure 8. Hydrogen production profiles of the Ti–Zr photocatalysts.

Among other factors, the reaction mechanism for any catalytic chemical transformation is related to the physicochemical properties of the catalyst. The presence of Zr into the titania lattice most likely modifies the reaction mechanism in our reaction system compared to that of pristine titania. A possible reaction mechanism for the water splitting and photooxidation of methanol in our Ti–Zr catalysts is the following. During the photocatalytic experiments, methanol could be activated on titanium and form an electron donor, as Guzman et al. have reported [37]. Although the authors studied the Cu/S-TiO_2 as a photocatalyst in the evolution of hydrogen from D_2O-methanol solutions, they found that the role of methanol is related to its ability to produce an electron donor injecting its electrons to the conduction band, and consequentially, increasing hydrogen production. A similar role of methanol is assumed in our study. Moreover, the existence of oxygen vacancies in the ZrO_2 lattice can capture these light-induced electrons from methanol, decreasing the oxidation state of zirconium ions. The oxidation state of zirconium ions can then be restored by the absorption of electron holes from the excited titania exposed to UV-irradiation, as it was previously reported for Ti–Mn photocatalysts [11]. The decrement in the band gap energies alone of the Ti–Zr samples compare to that of undoped titania was insufficient

to explain the hydrogen rates observed in our experiments. The positive effect of zirconium into titania can be explained by assuming that the presence of this metal retards the recombination of the light-induced electron and electron holes, increasing their possibilities to reach the catalytic surface to react with water. The final result would be an increase in the generation of hydrogen, as it was indeed observed experimentally. Other reports in the literature have also observed an enhancement in hydrogen production from water using sacrificial reactants [38]. In this work, Fontelles et al. studied the production of H_2 under visible and UV light, and in presence of niobium-doped and undoped titania using Pt as co-catalyst, and methanol, ethanol and 2-propanol as sacrificial reactants. The authors found that the synthetised catalysts showed similar morphological features and band gap values, and explained that the differences in activity were quantitatively correlated with the average oxidation potential of the alcohols, and concluded that thermodynamic of the interaction photocatalyst-sacrificial agent is likely driving the catalytic process.

To further study the stability of the TZr-10 catalyst, its photocatalytic activity was monitored during various reaction cycles. After the first run, the catalyst was washed with deionised water, dried for 8 h and calcined during 5 h at 500 °C. The sample was ready again to be evaluated in the generation of hydrogen as a photocatalyst. Following this treatment, the TZr-10 catalyst was tested during 4 cycles, and the measured hydrogen production is reported in Figure 9. The decrease in photocatalytic activity was probably due a change in the physicochemical properties of the sample resulted after consecutive calcinations.

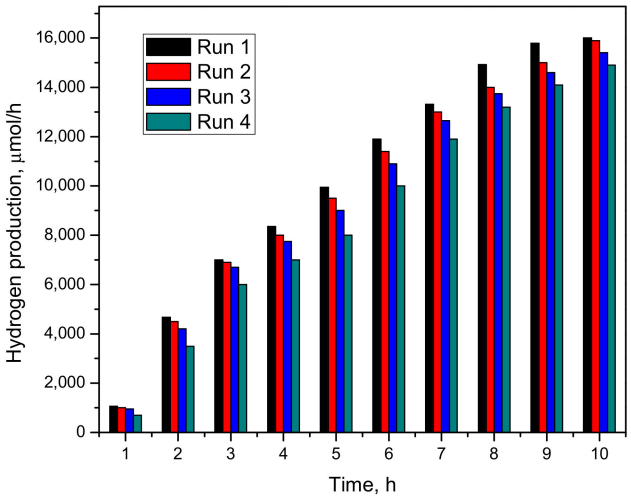

Figure 9. Photocatalytic activity of the TZr-10 sample in the generation of hydrogen from a methanol-water solution.

4. Experimental

4.1. Synthesis of Samples

The Ti–Zr samples were prepared by sol-gel using the required quantities of titanium (IV) butoxide ($C_{16}H_{36}O_4Ti$, 97%) and zirconium acetylacetonate ($C_{20}H_{28}O_8Zr$, 99%) to prepare oxides containing 1.0, 3.0, 5.0 and 10.0 wt.% of Zr. The metal compounds were dissolved in 44 mL of 1-butanol (99.4%) (reagents obtained from Sigma-Aldrich Chemical Co., St. Louis, Mo, USA), and 18 mL of dionized water under stirring and the pH of the solution was adjusted to 3 with an aqueous nitric-acid solution. The water/alkoxide molar ratio was 8. The solution was heated up to 70 °C and kept at this temperature for 24 h. During this period, the formation of a solid was observed. After this time the mixture was then cooled down to ambient temperature. The resulted solid was filtered and dried at 100 °C during 24 h. After this treatment, the samples were calcined at 500 °C during 5 h, applying a heating rate of 1 °C/min from ambient temperature to the set point. Pure titania was also prepared following similar procedure and was then used as a reference. The samples were then ready to be used as photocatalysts

in the splitting of water and for characterisation. The calcined binary oxides were designated as TZr-1, TZr-3, TZr-5, TZr-10 according to the weight per cent of zirconium.

4.2. Characterisation

The features of the catalysts were analysed by taken some micrographs using a scanning electron microscope (SEM) (Tescan, MIRA3 LMU, London, UK). The instrument is coupled with an EDS detector (Xfash sve 6/30, Bruker, Berlin, Germany) which allows the determination of the surface composition. The textural properties of the samples were evaluated by nitrogen adsorption–desorption isotherms which were obtained using a Quantachrome Autosorb 3B instrument (Quantachrome Instruments, Boynton Beach, FL, USA). Prior to nitrogen adsorption, all samples were outgassed at 200 °C for 5 h. The specific surface areas and the mean pore size diameter were then evaluated using the BET and BJH methods, respectively. X-ray diffraction (XRD) patterns of TiO_2 and Ti–Zr mixed oxides were acquired using a Bruker D-8 Advance apparatus (Kalsruhe, Germany). The diffraction intensity as a function of the diffraction angle was measured from 4° and 70° 2θ, using a step of 0.03° and a counting time of 0.3 s per step. Fourier transformed Raman spectra were collected using a Thermo Nicolet ALMEGA dispersive Raman spectrometer equipped with a diode-pumped solid state laser (Nd:YVO4) of 532 nm and operated at 25 mW. The beam was doubly focused on a sample placed in a capillary tube. The light scattered from the sample at 90° was focused at the entrance slit of a double monochromator and collected by a CCD detector connected to a computer. High-resolution gratings were used to give a spectral resolution of 2 cm^{-1}. The spectra were recorded at ambient temperature using 16 scans with an exposure time of 1 s per scan. For the acquisition of diffuse reflectance spectra, a UV–vis spectrophotometer (Shimadzu UV-2600, Tokio, Japan) provided with an integration sphere was used. A MgO sample was utilised as a reference. The surface composition of the catalysts and the chemical states of the elements were analysed by X-ray photoelectron spectroscopy (XPS) using a (Thermo Scientific K-Alpha, Tokyo, Japan) X-ray photoelectron spectrometer provided with a monochromatic Al Ka X-ray source of 1487 eV. Narrow scans were collected at Epass 60 eV with a spot size of 400 mm. To minimize the charge effects, the samples were supported on an indium foil. High resolution images were acquired using a high resolution transmission electron microscope, HRTEM, (Jeol microscope, JEM-ARM200F, Boston, MA, USA.) operated at 200 kV. The resulted images were analysed using Gatan Micrograph software v. 3.7.0. (Pleasanton, CA, USA).

The schematic reaction system used for testing the catalysts in the water splitting reaction was described in a previous work [12]. Briefly, it is a closed system containing a glass reactor provided with a UV-lamp, circulation pump, GC equipment and a water trap. Photocatalytic experiments allowing in situ determination of the hydrogen as function of reaction time were performed. The reactor is a modified Pyrex container of 200 mL which was filled with an aqueous methanol solution (1:1 M) and 0.1 g of catalyst. The irradiation was supplied using a high pressure Hg pen-lamp (Westbury, NY, USA) (254 nm and 2.2 mW/cm^2) encapsulated in a quartz tube which was then immersed in the aqueous methanol solution. The hydrogen generated was determined by gas chromatography using a Shimadzu GC-8 (Tokio, Japan) apparatus provided with a TCD and a 5A molecular sieve column (30 m long, 0.35 mm ID and 50 mm OD).

5. Conclusions

A series of Ti-Zr oxides were successfully prepared by sol-gel and then used as photocatalysts in the production of hydrogen from methanol–water solutions. Results from the characterisation indicate that increasing the Zr content in the titanium oxide resulted in the formation of bimetallic solid solutions. Furthermore, the specific surface areas increased compared to that of pure titania. The photocatalytic experiments showed that all Ti-Zr samples exhibited higher photocatalytic activities for the production of hydrogen than that observed for pristine titania. Hydrogen rates of 387, 900, 1600 and 2100 μmoL/h were measured for TZr-1, TZr-3, TZr-5 TZr-10 samples, whereas a value of 190 μmoL/h was determined for undoped titania. The positive effect of the incorporation of Zr into

titania could be explained by assuming that its presence retards the recombination of the light-induced electron and electron holes, resulting in a higher hydrogen production rates than that observed for undoped titania. Our results demonstrate the improvement of adding small quantities of Zr into the titanium lattice which leads to attractive photocatalysts for the generation of hydrogen from aqueous methanol solutions.

Author Contributions: R.G. designed and supervised the project; A.P.-L. performed the experiments and analyzed the data; J.L.R., L.M.A.-E., O.A.G.V. and N.G.-S. contributed with characterization of materials, analyzed the data and wrote the manuscript. All authors reviewed the manuscript before submission.

Funding: This research was funded by Conacyt through Grant No. 63053.

Acknowledgments: A. Pérez-Larios thanks Conacyt for the scholarship, and to Sergio Oliva and Martin Flores from CUCEI, University of Guadalajara, for the acquisition of SEM images.

Conflicts of Interest: The authors declare no conflict of interest.

References

1. Da Silva Veras, T.; Mozer, T.S.; Da Costa Rubim Messeder dos Santos, D.; Da Silva Cesar, A. Hydrogen: Trends, production and characterization of the main process worldwide. *Int. J. Hydrog. Energy* **2017**, *42*, 2018–2033. [CrossRef]
2. Ismail, A.A.; Bahnemann, D.W. Photochemical splitting of water for hydrogen production by photocatalysis: A review. *Sol. Energy Mater. Sol. Cells* **2014**, *128*, 85–101. [CrossRef]
3. Fujishima, A.; Honda, K. Electrochemical photolysis of water at a semiconductor electrode. *Nature* **1972**, *238*, 37–38. [CrossRef] [PubMed]
4. Bard, A.J.; Fox, M.A. Artificial photosynthesis: Solar splitting of water to Hydrogen and oxygen. *Acc. Chem. Res.* **1995**, *28*, 141–145. [CrossRef]
5. Chen, X.; Shen, S.; Guo, L.S.; Mao, S. Semiconductor-based photocatalytic hydrogen generation. *Chem. Rev.* **2010**, *110*, 6503–6570. [CrossRef] [PubMed]
6. Moriya, Y.; Takatab, T.; Domen, K. Recent progress in the development of (oxy) nitride photocatalysts for water splitting under visible-light irradiation. *Coord. Chem. Rev.* **2013**, *257*, 1957–1969. [CrossRef]
7. Wold, A. Photocatalytic properties of titanium dioxide (TiO_2). *Chem. Mater.* **1993**, *5*, 280–283. [CrossRef]
8. Hoffmann, M.R.; Martin, S.T.; Choi, W.; Bahnemannt, D.W. Environmental applications of semiconductor photocatalysis. *Chem. Rev.* **1995**, *95*, 69–96. [CrossRef]
9. Wang, M.; Shen, S.; Li, L.; Tang, Z.; Yang, J. Effects of sacrificial reagents on photocatalytic hydrogen evolution over different photocatalysts. *J. Mater. Sci.* **2017**, *52*, 5155–5164. [CrossRef]
10. Kumaravela, V.; Mathewa, S.; Bartletta, J.; Pillaia, S.C. Photocatalytic hydrogen production using metal doped TiO_2: A review of recent advances. *Appl. Catal. B Environ.* **2019**, *244*, 1021–1064. [CrossRef]
11. Pérez-Larios, A.; Hernández-Gordillo, A.; Morales-Mendoza, G.; Lartundo-Rojas, L.; Mantilla, A.; Gómez, R. Enhancing the H_2 evolution from water–methanol solution using Mn^{2+}–Mn^{+3}–Mn^{4+} redox species of Mn-doped TiO_2 sol—gel photocatalysts. *Catal. Today* **2016**, *266*, 9–16. [CrossRef]
12. Pérez-Larios, A.; Lopez, R.; Hernández-Gordillo, A.; Tzompantzi, F.; Gómez, R.; Torres-Guerra, L.M. Improved hydrogen production from water splitting using TiO_2–ZnO mixed oxides photocatalysts. *Fuel* **2012**, *100*, 139–143. [CrossRef]
13. Guerrero-Araque, D.; Acevedo-Peña, P.; Ramírez-Ortega, D.; Calderon, H.A.; Gómez, R. Charge transfer processes involved in photocatalytic hydrogen production over CuO/ZrO_2-TiO_2 materials. *Int. J. Hydrog. Energy* **2017**, *42*, 9744–9753. [CrossRef]
14. Yang, J.; Ferreira, J.M.F. On the Titania Phase Transition by Zirconia Additive in a Sol-Gel-Derived Powder. *Mater. Res. Bull.* **1998**, *33*, 389–394. [CrossRef]
15. Chang, S.; Doong, R. Characterization of Zr-Doped TiO_2 Nanocrystals Prepared by a Nonhydrolytic Sol-Gel Method at High Temperatures. *J. Phys. Chem. B* **2006**, *110*, 20808–20814. [CrossRef]
16. Gómez-Avilés, A.; Peñas-Garzón, M.; Bedi, J.; Dionysiou, D.D.; Rodríguez, J.J.; Belver, C. Mixed Ti-Zr metal-organic-frameworks for the photodegradation of acetaminophen under solar irradiation. *Appl. Catal. B Environ.* **2019**, *253*, 253–262. [CrossRef]

17. Daturi, M.; Cremona, A.; Milella, F.; Busca, G.; Vogna, E. Characterisation of Zirconia-Titania Powders Prepared by Coprecipitation. *J. Eur. Ceram. Soc.* **1998**, *18*, 1079–1087. [CrossRef]
18. Ohsaka, T.; Izumi, F.; Fujiki, Y. Raman spectrum of anatase. TiO_2. *J. Raman Spectrosc.* **1978**, *7*, 321–324. [CrossRef]
19. Kokporka, L.; Onsuratoom, S.; Puangpetch, T.; Chavadej, S. Sol-gel-synthesized mesoporous-assembled TiO_2–ZrO_2 mixed oxide nanocrystals and their photocatalytic sensitized H_2 production activity under visible light irradiation. *Mater. Sci. Semicond. Process.* **2013**, *16*, 667–678. [CrossRef]
20. Navarro Yerga, R.M.; Álvarez Galvan, M.C.; del Valle, F.; Villoria de la Mano, J.A.; Fierro, J.L. Water splitting on semiconductor catalysts under visible-light irradiation. *CHEMSUSCHEM* **2009**, *2*, 471–485. [CrossRef]
21. Butler, M.A. Photoelectrolysis and physical properties of the semiconducting electrode WO_2. *J. Appl. Phys.* **1977**, *48*, 1914–1920. [CrossRef]
22. Bak, T.; Nowotny, J.; Rekas, M.; Sorrell, C.C. Photo-electrochemical hydrogen generation from water using solar energy. Materials-related aspects. *Int. J. Hydrog. Energy* **2002**, *27*, 991–1022. [CrossRef]
23. Lin, W.-C.; Yang, W.-D.; Huang, I.-L.; Wu, T.-S.; Chung, Z.-J. Hydrogen Production from Methanol/Water Photocatalytic Decomposition Using $Pt/TiO_{2-x}N_x$ Catalyst. *Energy Fuels* **2009**, *23*, 2192–2196. [CrossRef]
24. Jeon, M.K.; Park, J.W.; Kang, M. Hydrogen production from methanol/water decomposition in a liquid photosystem using the anatase and rutile forms of Cu-TiO_2. *J. Ind. Eng. Chem.* **2007**, *13*, 84–91.
25. Guzman, F.; Chuang, S.S.C.; Yang, C. Role of Methanol Sacrificing Reagent in the Photocatalytic Evolution of Hydrogen. *Ind. Eng. Chem. Res.* **2013**, *52*, 61–65. [CrossRef]
26. Scherrer, P. Bestimmung der Grosse und der Inneren Struktur von Kolloidteilchen Mittels Rontgenstrahlen. *Nachr. Ges. Wiss. Göttingen* **1918**, *2*, 98–100.
27. Kernazhitsky, L.; Shymanovska, V.; Gavrilko, T.; Puchkovska, G.; Naumov, V.; Khalyavka, T.; Kshnyakin, V.; Chernyak, V.; Baran, J. Titanium-Manganese Oxides. Optical and Photocatalytic Properties. *Mater. Sci. Eng. B* **2010**, *175*, 48–55. [CrossRef]
28. Borchert, H.; Shevchenko, E.V.; Robert, A.; Mekis, I.; Kornowski, A.; Grübel, G.; Weller, H. Determination of Nanocrystal Sizes: A Comparison of TEM, SAXS, and XRD Studies of Highly Monodisperse $CoPt_3$ Particles. *Langmuir* **2005**, *21*, 1931–1936. [CrossRef]
29. Alivisatos, A.P. Perspectives on the Physical Chemistry of Semiconductor Nanocrystals. *J. Phys. Chem.* **1996**, *100*, 13226–13239. [CrossRef]
30. Roy, M.; Pompella, A.; Kubacki, J.; Piosik, A.; Psiuk, B.; Klimontko, J.; Szade, J.; Roy, R.A.; Hedzelek, W. Photofunctionalization of dental zirconia oxide: Surface modification to improve bio-integration preserving crystal stability. *Colloids Surf. B Biointerfaces* **2017**, *156*, 194–202. [CrossRef]
31. Avilés-García, O.; Espino-Valencia, J.; Romero-Romero, R.; Rico-Cerda, J.L.; Arroyo-Albiter, M.; Solís-Casados, D.A.; Natividad-Rangel, R. Enhanced Photocatalytic Activity of Titania by Co-Doping with Mo and W. *Catalysts* **2018**, *8*, 631. [CrossRef]
32. Li, J.; Li, B.; Li, J.; Liu, J.; Wang, L.; Zhang, H.; Zhang, Z.; Zhao, B. Visible-light-driven photocatalyst of La-N-codoped TiO_2 nano-photocatalyst: Fabrication and its enhanced photocatalytic performance and mechanism. *J. Ind. Eng. Chem.* **2015**, *25*, 16–21. [CrossRef]
33. Lin, G. Hierarchically macro–mesoporous ZrO_2–TiO_2 composites with enhanced photocatalytic activity. *Ceram. Int.* **2015**, *41*, 575–5749.
34. Linnik, O.; Shestopal, N.; Smirnova, N.; Eremenko, A.; Korduban, O.; Kandyba, V.; Kryshchuk, T.; Socol, G.; Stefan, N.; Popescu-Pelin, G.; et al. Correlation between electronic structure and photocatalytic properties of non-metal doped TiO_2/ZrO_2 thin films obtained by pulsed laser deposition method. *Vacuum* **2015**, *114*, 166–171. [CrossRef]
35. Foster, A.S.; Sulimov, V.B.; Gejo, F.L.; Shluger, A.L.; Nieminen, R.M. Structure and electrical levels of point defects in monoclinic zirconia. *Phys. Rev. B Condens. Matter* **2001**, *64*. [CrossRef]
36. Youssef, M.; Yildiz, B. Intrinsic point-defect equilibria in tetragonal ZrO_2: Density functional theory analysis with finite-temperature effects. *Phys. Rev. B* **2012**, *86*. [CrossRef]

37. Ma, W.; Herbert, F.W.; Senanayake, S.D.; Yildiz, B. Non-equilibrium oxidation states of zirconium during early stages of metal oxidation. *Appl. Phys. Lett.* **2015**, *106*. [CrossRef]
38. Fontelles-Carceller, O.; Muñoz-Batista, M.J.; Rodríguez-Castellón, E.; Conesa, J.C.; Fernández-García, M.; Kubacka, A. Measuring and interpreting quantum efficiency for hydrogen photo-production using Pt-titania catalysts. *J. Catal.* **2017**, *347*, 157–169. [CrossRef]